JOURNAL OF MATERIALS SCIENCE 28 (1993) 3722–3730

Energy absorption mechanisms during dynamic fracturing of fibre-reinforced composites

S. K. KHANNA, A. SHUKLA
Dynamic Photomechanics Laboratory, Department of Mechanical Engineering and Applied Mechanics, University of Rhode Island, Kingston, RI 02881, USA

Dynamic photoelastic experiments were conducted to study crack propagation in fibre-reinforced materials and, in particular, to determine the energy losses occurring during the crack growth and arrest process. This study utilized modified compact tension specimens which were fabricated from polyester matrix and different reinforcing fibres. The effect of the fibre-matrix interface on energy absorbed was also studied. The energy absorbed was partitioned into two parts: that absorbed in the fracture process zone associated with the crack tip, and the energy lost outside this zone. Results show that fibre reinforcement reduces the energy absorbed in the fracture process zone by about 10% for well-bonded and 15% for partly debonded fibres. For the same initial strain energy, this reduction in fracture energy manifests itself in reduced K_{ID} and lower crack-jump distance as compared to monolithic specimens. Reinforced specimens are found to retain a higher strain energy after crack arrest. The energy absorbed outside the fracture process zone for monolithic and well-bonded fibres is about 45% of the initial strain energy, while for partly debonded fibres it is about 55%.

1. Introduction

In any fracture event, the growth of a crack is driven by the crack-driving force and opposed by the resistance of the microstructure. The resistance to crack growth stems from those fracture mechanisms which absorb energy during fracture and from those mechanisms which can dissipate and/or absorb energy outside the fracture process zone.

It has been shown experimentally [1, 2] that in Homalite-100, a polyester material, approximately 40% of the initial strain energy is lost due to damping during rapid crack propagation and after arrest in a modified compact tension (MCT) specimen. The rest of the energy is absorbed as surface energy during formation of new crack surfaces or retained as strain energy in the system after arrest. However, when continuous fibres are used in materials, several other energy-absorbing mechanisms are introduced. These mechanisms can be microcracking in the fracture process zone, fibre debonding, fibre breakage, fibre pull-out and crack-face bridging by unbroken fibres. Energy can also be dissipated by emission of low-amplitude stress waves when microcracks are formed in the fracture process zone and by damping after crack arrest when the kinetic energy is continuously converted to strain energy and vice versa. These mechanisms are important as they increase the crack-growth resistance of the composite. The effect of these mechanisms on incremental crack growth in fibre-reinforced brittle-matrix composites has been studied using the stress-intensity approach by Marshall *et al.* [3], Bowling and Groves [4, 5] and Rose [6]. At the same time, the energy approach has been pursued by Jenkins *et al.* [7] and Wells and Beaumont [8]. The effect of the fibre–matrix interface and the stress state occurring at the interface has a profound effect on the fracture behaviour of the composite. The effect of interface debonding and the residual stress state at the interface on crack-growth resistance has been studied by Sigl and Evans [9], Cao and Evans [10], and Charalambides and Evans [11]. The effect of the interface on the stress-intensity factor and crack-closing forces by bridging fibres during dynamic crack propagation has been investigated by Shukla and Khanna [12].

This paper describes a series of experiments conducted with a birefringent polyester reinforced with nickel fibres, copper fibres and E-glass fibre strands to determine the relative amounts of energy dissipated during the rapid crack growth and arrest event. In order to obtain optically transparent specimens and to be able to concentrate on the effect of each fibre on the crack propagation and arrest process, the fibre volume fraction was kept very low, of the order of 0.2%. The fibre volume fraction hereon is referred to as the fibre spacing. Two regions have been identified in which energy is absorbed and dissipated: one is the fracture process zone associated with the crack tip, second is the region outside this zone. The energy associated with the fracture process zone is termed the fracture energy, E_f, and the energy dissipated outside this zone is designated by E_d. The fracture mechanisms occurring in the fracture process zone are microcrack initiation, fibre debonding and/or breakage. In the wake of the crack, unbroken fibres continue to debond and also bridge the crack faces. As the load on these

0022–2461

fibres increases, so does the elastic strain energy stored in the fibre and the matrix. These bridging fibres apply closing forces on the crack faces and can restrain the crack-opening displacement and reduce the crack-tip stresses. If the bridging fibres break, the energy in the debonded region will be dissipated as heat and by stress-wave emission. Energy is also absorbed by the formation of new debonded surfaces. Failure of the debonded fibres results in pull-out, resulting in energy dissipation due to work done against interfacial friction.

This experimental study utilizes a balance of energy approach in the system [1], given by

$$U_i - U_f = E_f + E_d \quad (1)$$

where U_i is the initial strain energy in the system, U_f the final strain energy after crack arrest and ring down, E_f the fracture energy, and E_d the dissipated energy. Equation 1 implies a fixed grip condition, that is no energy was added or removed from the fracture specimen during the run arrest event. This boundary condition was attained in the loading system used and the displacement of the loading members was monitored during the run arrest event to ensure the achievement of fixed grip condition in practice.

2. Experimental procedure

2.1. Specimen and loading fixture

The fracture specimen used in these experiments was a modified compact tension (MCT) specimen shown in Fig. 1. This type of specimen ensures rapid crack growth followed by crack arrest even for high values of K_Q, where K_Q is the initiation stress-intensity factor associated with a blunt crack tip. The specimens were fabricated from plates obtained by the following procedure. Nickel fibres (250 μm diameter), copper fibres (250 μm diameter) or E-glass fibre strands consisting of fibres of 10 μm diameter were wound on a rectangular metal frame at the required spacing. The frame was then pressed between two thick plexiglass plates lined with mylar sheets, to form the mould for casting the composite plate about 12 mm thick. Clear-grade polyester resin MR17090 (Airistech Chemical Corporation) mixed with 0.85% by weight methyl ethyl ketone peroxide and 0.3% by weight of cobalt octoate, was poured into the mould and allowed to cure at room temperature for 1 day. The plate was later post-cured at 55 °C for 18 h followed by 80 °C for 6 h and then allowed to cool slowly in the oven. Different fibre–matrix interface conditions were obtained by coating the fibres with release agent containing modified polysiloxane polymers and trichloroethene dissolved in hydrocarbon propellants before casting.

The specimen was loaded with a transverse wedge and a split D which is shown in Fig. 2. The loading wedge is behind the displacement transducer and so is not visible in Fig. 2. The wedge was pulled between the two split Ds with a hydraulic cylinder. The split Ds were fitted in the circular hole in the MCT specimen. After the specimen was loaded to the desired value of K_Q or U_i the wedge was locked into a fixed position with the locking screw. Also two stops were placed along the loading line on the outer edges of the specimen to prevent any outward displacement during the propagation and arrest event. Relative displacement of the split Ds was monitored with an eddy current transducer before and after the event.

2.2. Strain-energy determination

The initial strain energy, U_i, was determined from the relation

$$U_i = \int_0^s P \, d\delta \quad (2)$$

which is the area under the load–displacement curves for the MCT specimens with the initial crack length, a_0. To determine U_i, the relation between the load, P,

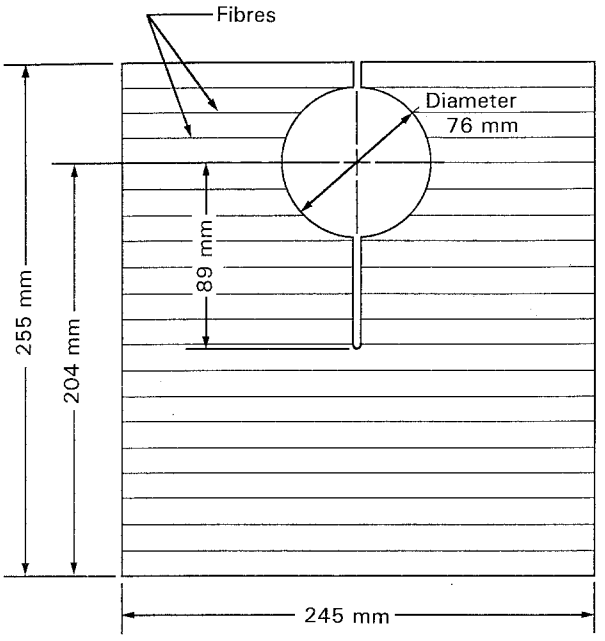

Figure 1 Fibre-reinforced modified compact tension specimen geometry. Specimen thickness = 12 mm.

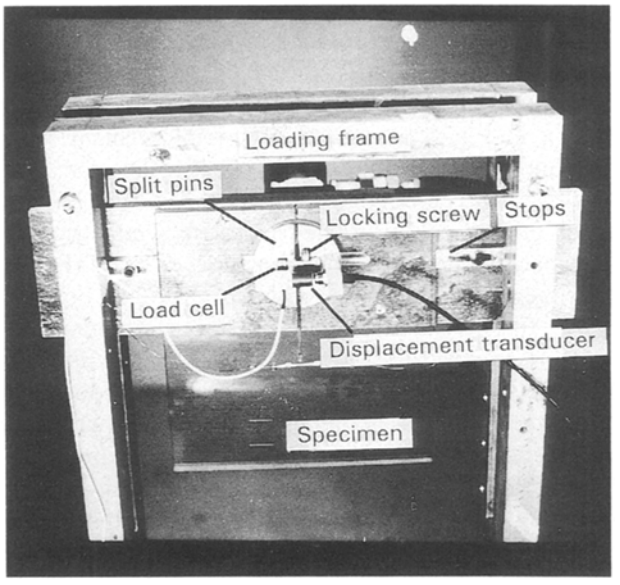

Figure 2 Loading fixture with the specimen.

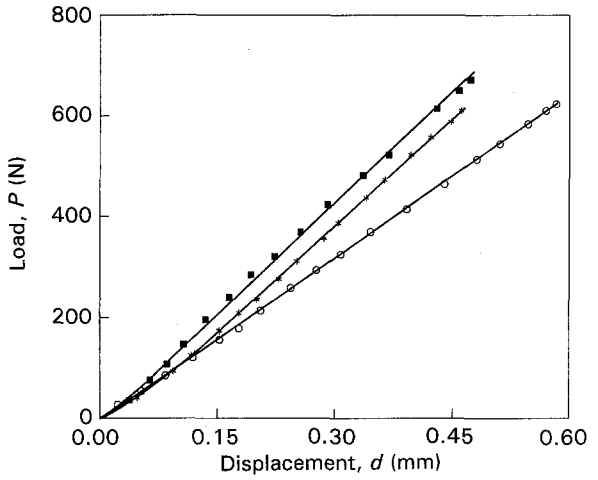

Figure 3 Typical load–displacement plots for nickel fibre-reinforced specimens. (∗) Monolithic (M-1), (■) well-bonded nickel fibres (N-4), (○) partly debonded nickel fibres (N-6).

and the relative displacement between the split D's, s, was established with a compliance calibration. The load, P, was measured with a quartz load cell positioned between the wedge and the split D fixture. The displacement s, was measured with an eddy current transducer which bridged the gap between the split D's. Typical load–displacement plots are shown in Fig. 3. Accuracies of 0.005 mm and 5 N were achieved in the determination of s and P, respectively. The final strain energy, U_f, was also determined by using Equation 2, i.e. by measuring the area under the load–displacement curve obtained with specimen containing the arrested crack of crack length, a_f.

2.3. Dynamic photoelastic experiments

Dynamic photoelastic experiments were performed with several fibre reinforced and a monolithic MCT specimen, each containing an initial crack $a_o/w = 0.437$. The specimens were loaded to a preselected value of K_Q and the crack was initiated by pulling a sharp knife across the blunt crack tip. As the crack began to propagate, it cut a line of silver-conducting paint and triggered a multiple spark Cranz–Schardin camera. The camera provided 20 isochromatic photographs at discrete times during the run arrest event. Typical isochromatic fringe patterns obtained are shown in Fig. 4 for nickel fibre-reinforcement with varying interface conditions and fibre inclination. For the case of well-bonded fibres perpendicular to the crack-growth direction, the fringes are symmetric but lean backwards, as in double cantilever beam (DCB) specimens. In specimens with very weakly bonded fibres, the fringes are symmetric about the crack tip and the backward leaning is very little. This implies that the weakly bonded fibres significantly reduce the component of stress acting in the plane of the crack in a direction opposite to the crack-growth direction. When the fibres are inclined to the crack-growth direction, the fringes are backward leaning but asymmetric about the crack tip. This suggests that the crack should grow along a curved path. However, the crack is found to grow along a straight line and also K_{IID} is very close to zero. This confirms the hypothesis that under dynamic conditions the crack grows under Mode I conditions even if the far-field stress is in mixed mode.

3. Analysis and results

The initial strain energy, U_i, in the specimen was determined by integrating the area under the load–displacement curve shown in Fig. 3, according to Equation 2. The final strain energy, U_f, was determined in the same manner by blunting the arrested crack tip and reloading the specimen.

The MCT fracture specimen ensures a rapid crack growth followed by an arrest. The crack length as a function of time can be determined from the isochromatic fringe patterns obtained at discrete times. Fig. 5 shows a typical plot of crack length as a function of time. The crack velocity is found to be constant for most of the crack-growth distance except near the arrest point where it rapidly slows down.

The fracture energy, E_f, was obtained from the photographs of the isochromatic fringe patterns. The dynamic stress field around a crack tip can be represented as a series [13]. The coefficients of this series were found by using the isochromatic fringes around the crack tip and the multiple-point least-squares method [14]. The dynamic stress intensity factor, K_{ID}, values thus obtained for nickel fibre-reinforcement are shown in Fig. 6 and for copper and glass fibre reinforcement in Fig. 7, as a function of the crack length to width ratio, a/w. The energy, E_f, was determined from the relation

$$E_f = A(v)\frac{h}{E_{dy}}\int_{a_o}^{a_f} K_{ID}^2(x)\,dx \qquad (3)$$

where $A(v)$ is the dynamic correction factor, h the specimen thickness, E_{dy} the dynamic modulus of the matrix, a_o the initial crack length, and a_f the final crack length. Results for the experiments conducted with nickel, E-glass and copper fibre-reinforced specimens are presented in Tables I–III, respectively.

4. Discussion

Dynamic fracture experiments with fibre-reinforced MCT specimens show that fibre reinforcement and the fibre–matrix interface changes the mode of crack–fibre interaction, affects the energy absorption and dissipation, and also the crack-jump distance in the composite.

4.1. Crack-fibre interaction

Fig. 8 shows the fracture surfaces obtained with nickel fibre reinforcement for various fibre–matrix interface conditions. The nature of the crack–fibre interaction during dynamic crack propagation is found to be similar to that proposed elsewhere [12]. When a crack front hits a fibre, the portion of the front immediately in front of the fibre tends to stop because of the higher toughness of the fibre. The original crack front divides into two fronts, on either side of the fibre, which

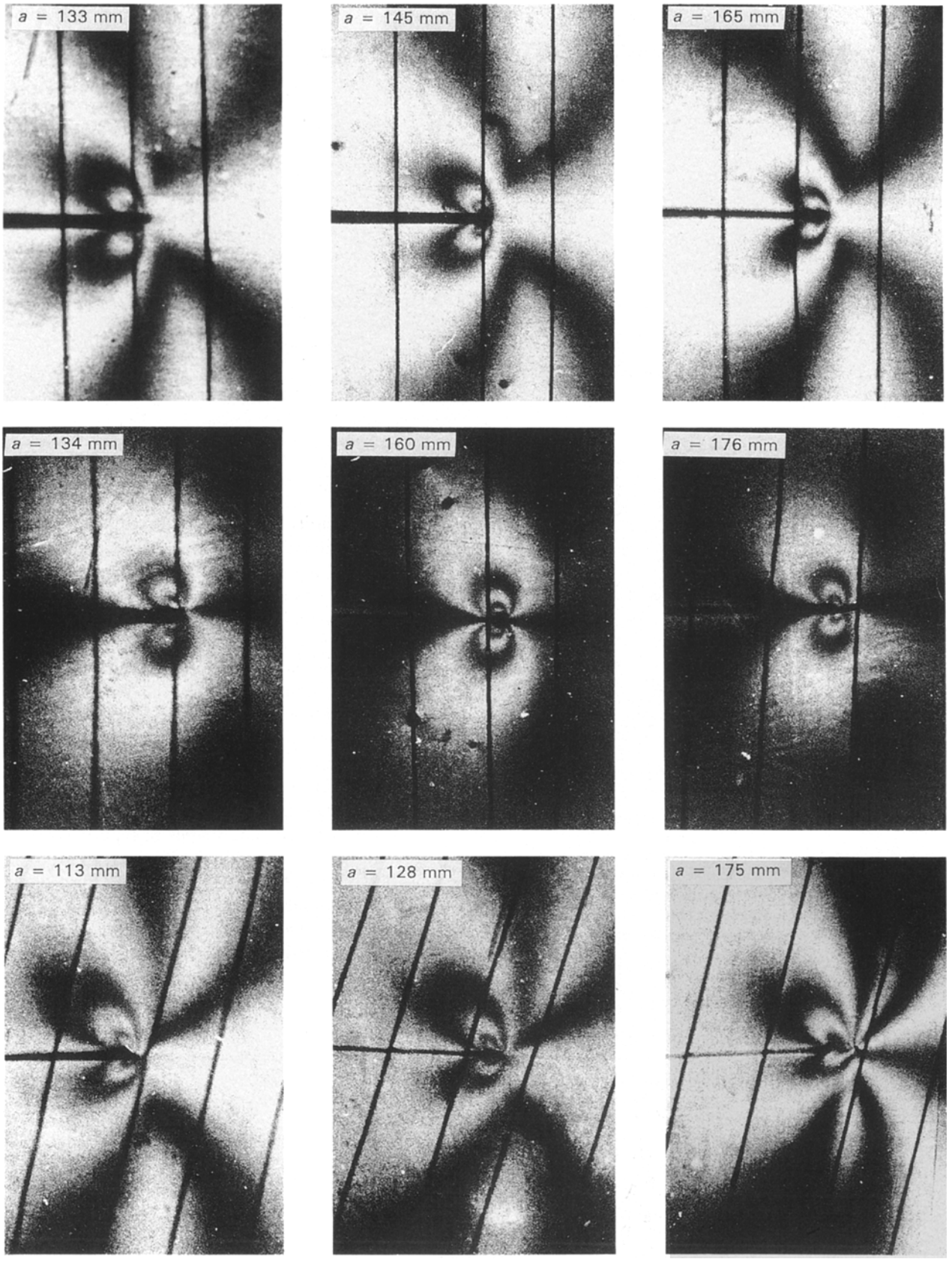

Figure 4 Typical isochromatic fringe patterns associated with a running crack in nickel fibre-reinforced specimens with 6.3 mm fibre spacing. Top row, well-bonded fibres; middle row, very weakly bonded fibres; bottom row, well-bonded fibres inclined at 15° to crack path.

advance slowly around the fibre producing a debonded zone along the fibre circumference and also along the length of the fibre. Now the crack front immediately in front of the fibre moves forward along the fibre circumference. However, it encounters an increasing projected area of the fibre and tends to stop again. This stop and go motion of the two crack fronts produces the thumb-nail shape marks on either side of the fibre, as seen in Fig. 8. In the case of a well-bonded fibre, the fibre presents a very high toughness to the moving crack and does not instantly debond as the divided fronts advance. Thus the portion of the crack

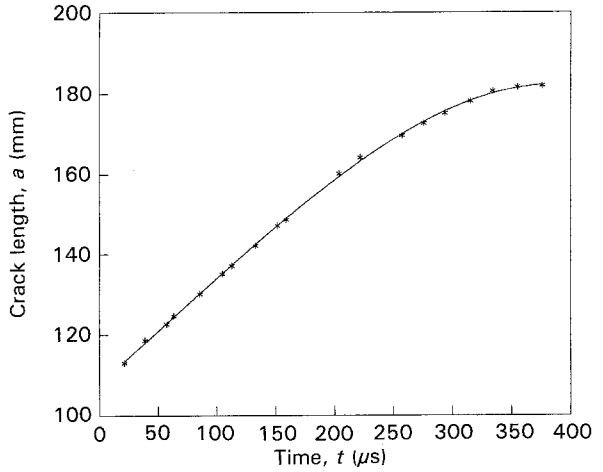

Figure 5 Typical plot of crack length as a function of time for fibre-reinforced MCT specimens.

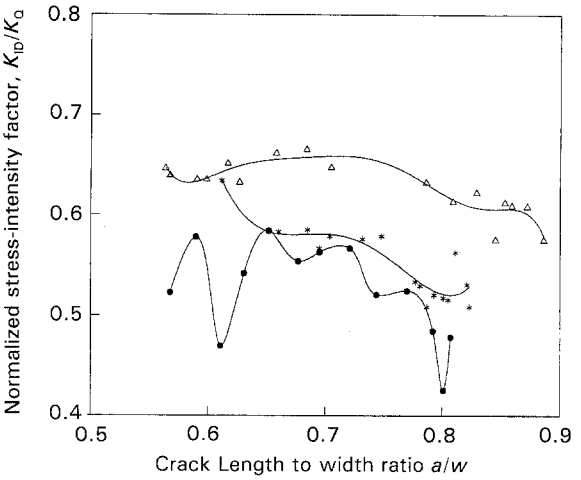

Figure 7 Dynamic stress intensity factor as a function of crack length to width ratio for copper fibres and E-glass fibre-reinforced specimens with 6.3 mm fibre spacing. (△) Monolithic (M-1), (∗) well-bonded copper fibres (C-2), (●) well-bonded glass fibres (G-1).

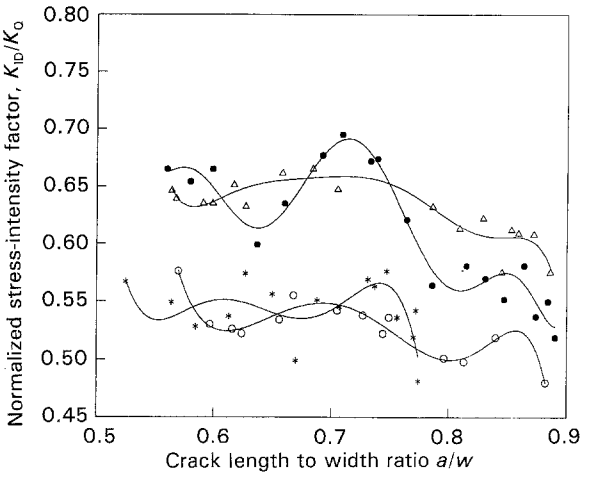

Figure 6 Dynamic stress intensity factor as a function of crack length to width ratio for monolithic and nickel fibre-reinforced specimens with 6.3 mm fibre spacing and various fibre–matrix interface conditions. (△) Monolithic (M-1), (∗) well-bonded fibres (N-2), (○) partly debonded fibres (N-6), (●) completely debonded fibres (N-5).

front in the vicinity of the fibre tends to slow down, producing the thumb-nail marks seen in Fig. 8a. For the completely debonded fibre, when the crack front hits the fibre it divides into two fronts and the fibre instantaneously debonds from the matrix as the interfacial strength is very low. The low interfacial shear strength also does not allow any significant crack-face bridging. As a consequence of the extensive fibre debonding and limited crack-face bridging, the divided crack fronts move at the same speed as that of the original front and hence the absence of the thumb nail marks in Fig. 8c. The divided fronts move to the end of the fibre where they rejoin, resulting in the formation of the step. The shapes of typical arrested crack fronts are shown in Fig. 9. The front seems to be pinned down by the fibres and the shape of this front is similar to the thumb-nail marks on either side of the fibre in Fig. 8a. The partially debonded fibres are more effective in reducing the fracture energy as they

TABLE I Results with nickel fibre (250 μm diameter) reinforced specimens

Expt.	Description (fibre spacing, interface state)	Crack jump (mm)	K_Q (MPa m$^{1/2}$)	U_i (J)	U_f (J)	E_f (J)	E_d (J)	E_f as % of U_i	E_d as % of U_i
M-1	Monolithic	91	0.83	0.140	0.005	0.072	0.063	51	45
N-1	12.5 mm, well-bonded	87	0.91	0.145	0.013	0.067	0.065	46	45
N-2	6.3 mm, well-bonded	68	0.89	0.125	0.023	0.043	0.059	34	47
N-3	6.3 mm, well-bonded	78	0.94	0.137	0.019	0.060	0.058	43	42
N-4	6.3 mm, well-bonded	91	1.03	0.159	0.011	0.070	0.078	44	49
N-5	6.3 mm, debonded	93	0.91	0.157	0.005	0.083	0.069	53	44
N-6	6.3 mm, debonded over ± 30 mm	90	0.96	0.181	0.018	0.062	0.101	34	56
N-7	6.3 mm, well-bonded, 15° fibre angle	85	0.95	0.144	0.015	0.065	0.064	45	44

TABLE II Results with E-glass fibre strand-reinforced specimens

Expt.	Description (fibre spacing, interface state)	Crack jump (mm)	K_Q (MPa m$^{1/2}$)	U_i (J)	U_f (J)	E_f (J)	E_d (J)	E_f as % of U_i	E_d as % of U_i
M-1	Monolithic	91	0.83	0.140	0.005	0.072	0.063	51	45
G-1	6.3 mm, well-bonded	75	1.03	0.192	0.019	0.079	0.094	41	49
G-2	6.3 mm, well-bonded	70	0.96	0.176	0.029	0.072	0.075	41	43

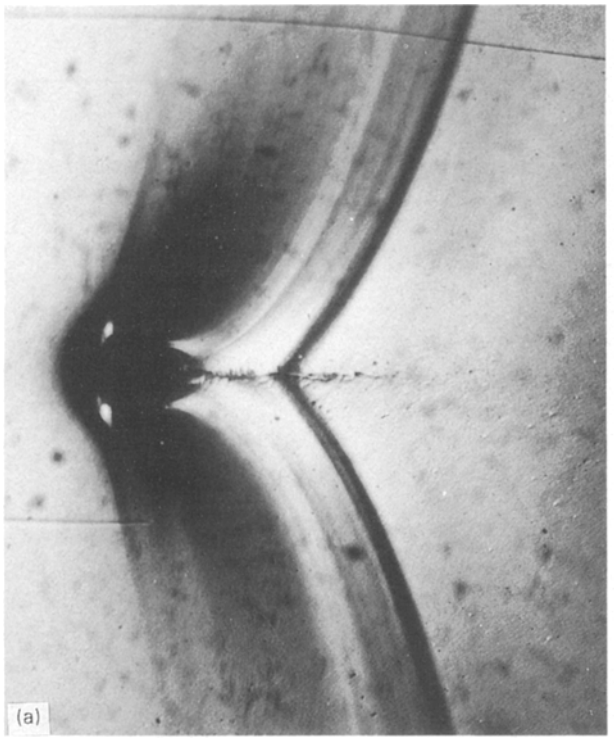

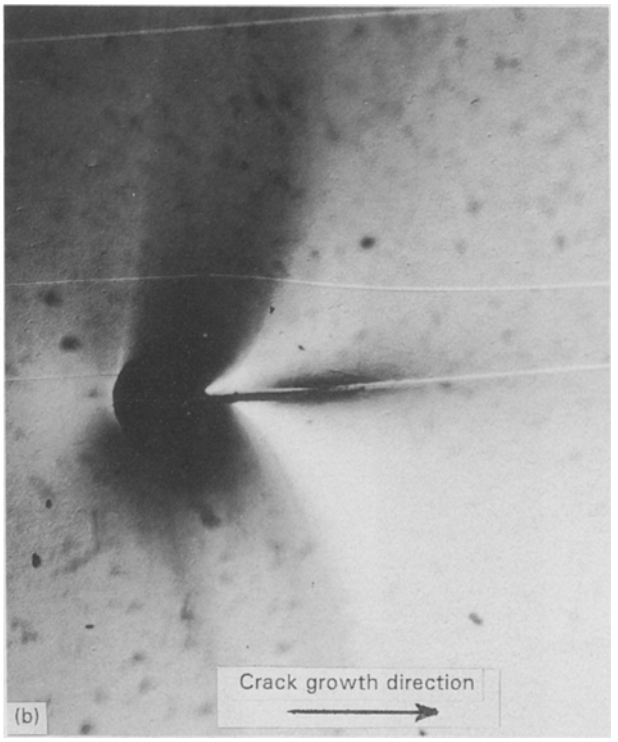

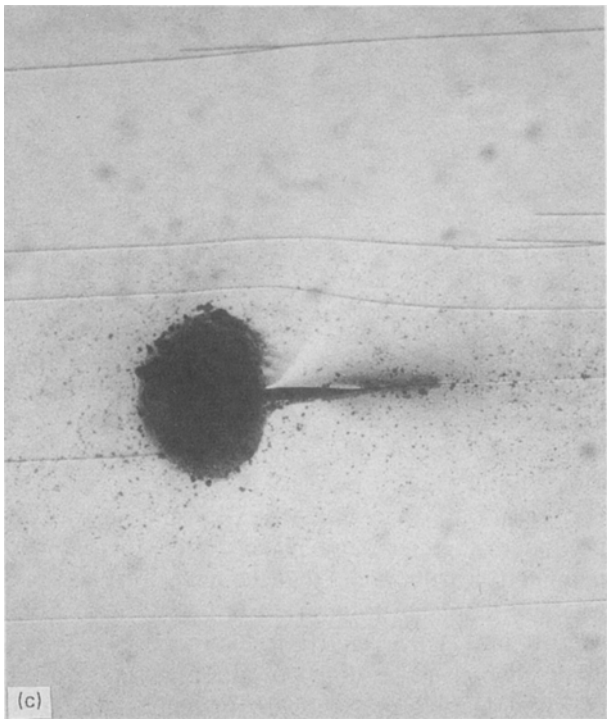

Figure 8 Fracture surface photographs for nickel fibre-reinforcement with 6.3 mm fibre spacing and various fibre–matrix interface conditions. (a) Well-bonded fibre, X5; (b) partly debonded fibre, X5; (c) completely debonded fibre, X5.

can debond rapidly to a certain length, which provides the gauge length over which they can stretch and apply closing forces on the crack faces. It has been shown elsewhere [12] that these forces are larger and become active earlier compared to those with well-bonded fibres. Thus the partly debonded fibres are able to reduce the crack-tip stresses while at the same time store more elastic strain energy.

4.2. Effect of reinforcement on crack-jump distance

Table I shows that for nickel fibre-reinforcement the crack jump distances are lower than in monolithic specimen even for initial K_Q 7%–25% higher. Table III shows that the crack-jump distance with copper fibre-reinforcement is lower compared to that in monolithic specimen for nearly the same initial K_Q, with the strain energy, U_i, being also close to that in the monolithic specimen. E-glass fibre strands are found to be very effective in reducing crack-jump distance, see Table II, as compared to both monolithic and nickel and copper fibre-reinforced specimens. Fig. 10 shows the crack-jump distance as a function of the initial strain energy per unit volume. The effectiveness of glass fibre-reinforcement in reducing crack jump is clear, with the jump distance being lower

TABLE III Results with copper fibre (250 μm diameter) reinforced specimens

Expt.	Description (fibre spacing, interface state)	Crack jump (mm)	K_Q (MPa m$^{1/2}$)	U_i (J)	U_f (J)	E_f (J)	E_d (J)	E_f as % of U_i	E_d as % of U_i
M-1	Monolithic	91	0.83	0.140	0.005	0.072	0.063	51	45
C-1	12.5 mm, well-bonded	90	0.86	0.131	0.117	0.065	0.059	50	45
C-2	6.3 mm, well-bonded	80	0.90	0.155	0.017	0.059	0.079	38	51
C-3	6.3 mm, well-bonded	78	0.89	0.141	0.019	0.055	0.067	39	48
C-4	6.3 mm, well-bonded 15° fibre angle	80	0.93	0.150	0.019	0.061	0.070	41	47

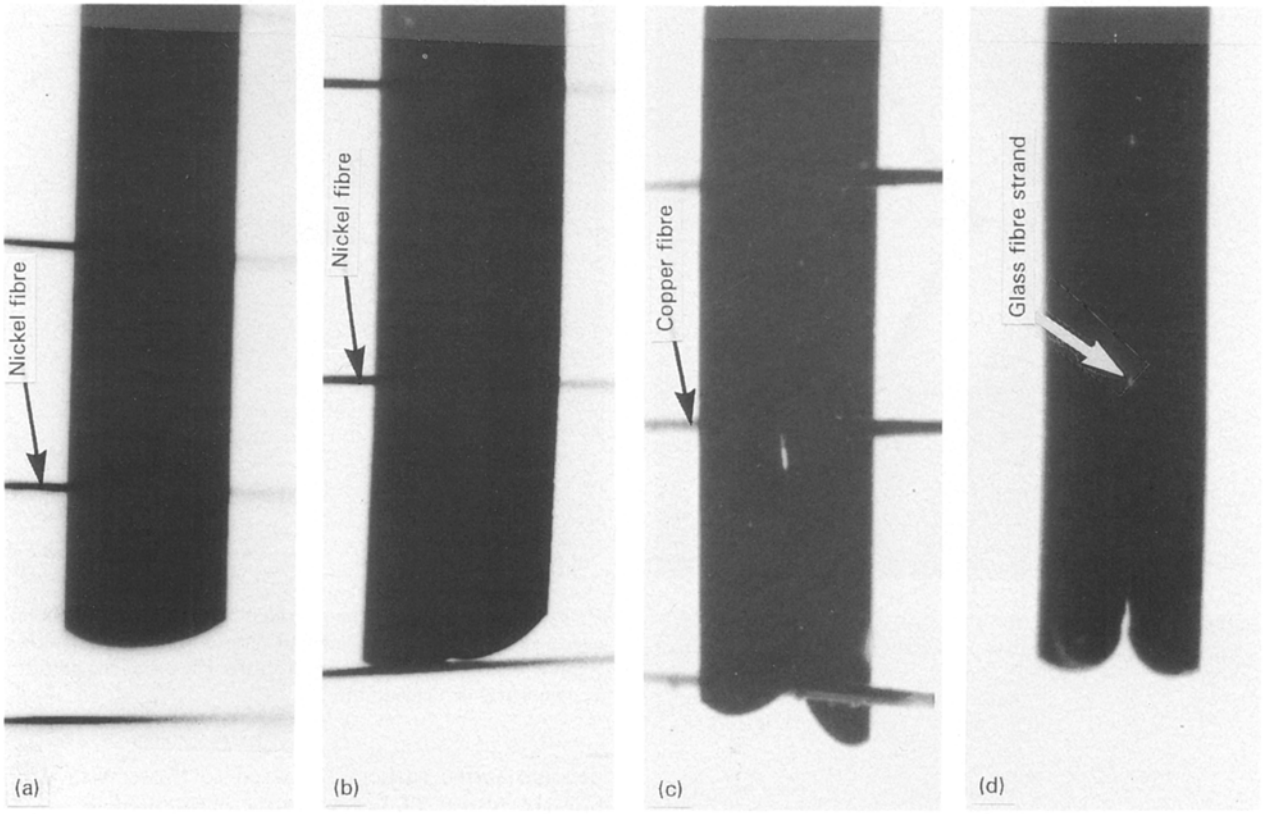

Figure 9 Various shapes of the arrested crack front in fibre-reinforced MCT fracture specimens, with the crack arrest occurring (a) in between two nickel fibres, (b) at a nickel fibre, (c) at a copper fibre, (d) at a glass fibre strand.

inspite of the larger U_i. When a crack grows in a fibre-reinforced specimen, the fibres continue to debond in the wake of the crack. The debonded length for well-bonded glass fibres is of the order of 5 mm. The debonded length for nickel and copper fibres is about 15 mm for well-bonded fibres and 60 mm for partly debonded fibres. The debonded length is influenced by the nature of the interfacial stress field. Compressive residual stresses develop at the interface of glass fibres, after post-curing, as the thermal expansion coefficient of glass is lower than that of the polyester matrix and tensile residual stresses develop at the interface in nickel and copper fibres as their thermal expansion coefficient is higher than that of the matrix. The crack-opening displacement depends on the extent of debonding in each type of fibre as the debonding changes the compliance of the system. The ratio of the crack-opening displacement to debonded length is the strain in the fibre [12]. It is plausible that the strain in the well-bonded glass fibres is sufficiently higher than nickel and copper fibres to result in larger closing forces being applied by glass fibres. This is possible because no appreciable plastic deformation was noticed in the copper and nickel fibres after the experiments, which implies that the strain in these fibres was less than the yield strain of 0.2%. Glass fibres deform in a linear elastic fashion and break at a relatively high strain of 5% or at a breaking strength of 3500 MPa. Hence, though no appreciable glass fibre breakage was noticed, these fibres can sustain high strains and thus apply large crack-closing forces.

The lowering of the crack-jump distance signifies that less energy is available for driving the crack. This is clearly seen in the reduction of fracture energy, E_f,

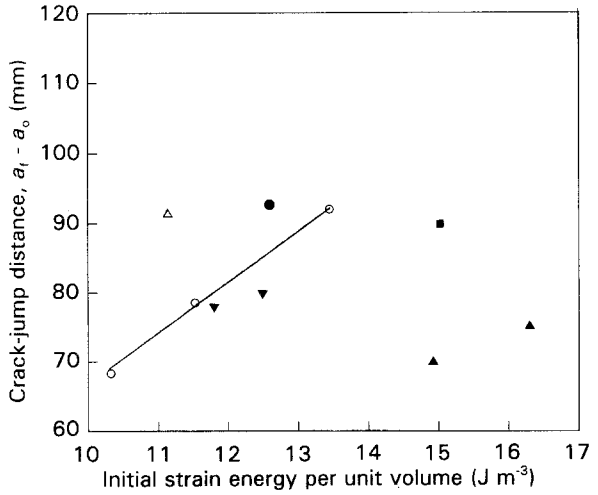

Figure 10 Crack-jump distance as a function of the initial strain energy per unit volume. (△) Monolithic, (○) well-bonded nickel fibres, (●) completely debonded nickel fibres, (■) partly debonded nickel fibres, (▼) well-bonded copper fibres, (▲) well-bonded glass fibres.

for all types of reinforcement with 6.3 mm fibre spacing, when compared with that of monolithic specimen. Specimens with well-bonded fibres are found to result in a reduction in E_f of about 8%–12%. However, the energy dissipated outside the fracture process zone is found to be comparable to that in the monolithic specimen. This is possibly due to the very low fibre-volume fraction, which does not allow any appreciable fibre breakage and pull-out, the latter being a major energy-dissipating mechanism. Nevertheless, fibres continue to debond in the wake of the crack and bridge the two crack faces. These bridging fibres apply closing forces on the crack faces and store elastic strain energy in the fibre and the matrix in the debonded region. This results in reduction in the fracture energy, while the final strain energy stored in the specimen after crack arrest increases when compared to the monolithic case.

4.3. Effect of fibre-matrix interface on energy absorption

The effect of the fibre–matrix interface on the crack growth and arrest process for nickel fibre-reinforcement was also studied. Three types of interfaces were studied, namely, well-bonded, debonded partially over a distance of 30 mm on either side of the fibre centre, and completely debonded over the entire length of the fibre. The well-bonded fibres, as discussed above, result in the reduction of the crack-jump distance, lowering in the fracture energy, and increase in the final strain energy, while there is no appreciable change in the dissipated energy. The completely debonded fibres result in an increase of the fracture energy and the crack-jump distance, as compared to specimens with well-bonded fibres. Thus the completely debonded fibres, as shown in Fig. 11, are not suitable for controlling dynamic crack growth in composites. The partially debonded fibres show a greater effectiveness in increasing resistance to crack growth. Fig. 12 shows the extent of debonding in well-bonded and partly

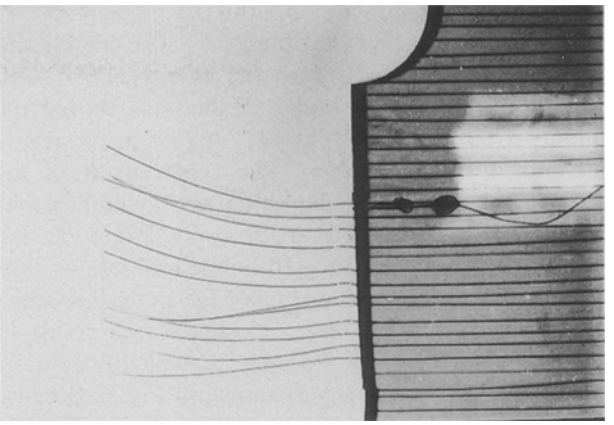

Figure 11 Figure showing completely debonded nickel fibres pulled out by gently separating the two sides of the cracked specimen.

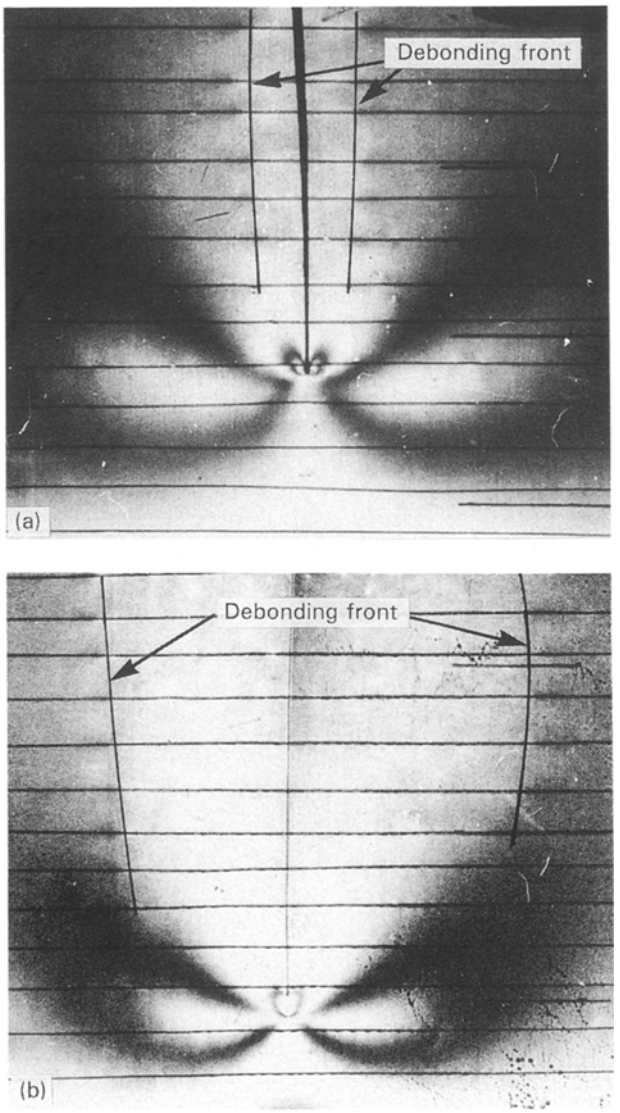

Figure 12 Figure showing debonding front along the fibre length for (a) well-bonded fibres, (b) fibres very weakly bonded over ± 30 mm on either side of the centre.

debonded fibres. Experiment N-6, Table I, shows that the reduction in fracture energy is 17% compared to monolithic specimen, 19% as compared to that with completely debonded fibres and about 10% with respect to well-bonded fibres. The crack-jump distance

is the same as that in a monolithic specimen inspite of a 16% higher K_Q and 28% higher U_i. The crack-jump distance when compared to the specimen N-4 with well-bonded fibres is found to be the same, though the initial strain energy, U_i, is 14% higher in the partly debonded fibre specimen. The achievement of the same crack jump for higher initial energy implies that the partially debonded fibres apply larger closing forces as compared to well-bonded fibres, as was shown elsewhere for the single-edge notch specimen geometry [12]. The larger closing forces result in reduction of the crack-tip stresses, which eventually shows up in reduced K_{ID} as shown in Fig. 6. Because partly debonded fibres debond over a significantly longer length, as shown in Fig. 12, the dissipated energy is found to be higher for this specimen. The fibre debond length is high in the case of very weakly bonded fibres, experiment N-5, but because the interface strength is very low, there is no significant energy dissipation. Thus, the dissipated energy still remains the same as for the monolithic specimen.

5. Conclusion

Photoelastic experiments of dynamic fracture with fibre-reinforced modified compact tension specimens show that reinforcement helps to reduce the crack-jump distance as compared to monolithic specimens for the same initial strain energy. In fibre-reinforced specimens the fracture energy associated with the process zone of the crack tip is reduced and the strain energy retained in the specimen after crack arrest increases. The fibre–matrix interface condition has a significant effect on energy absorption and crack-jump distance. Fibres with a weak interface in the vicinity of the dynamic crack tip are more effective in reducing fracture energy and crack jump, as compared to fibres with a stronger fibre–matrix interface.

Acknowledgements

The support of the National Science Foundation under grant INT-9011088 is greatfully acknowledged. The authors thank Airistech Chemical Corp. for sup plying the polyester resin.

References

1. J. W. DALLY and A. SHUKLA, *Eng. Fract. Mech.* **13** (1980) 807.
2. A. SHUKLA and W. L. FOURNEY, *ibid.* **19** (1984) 251.
3. D. B. MARSHALL, B. N. COX and A. G. EVANS, *Acta Metall.* **33** (1985) 2013.
4. J. BOWLING and G. W. GROVES, *J. Mater. Sci.* **14** (1979) 431.
5. *Idem, ibid.* **14** (1979) 443.
6. L. R. F. ROSE, *J. Mech. Phys. Solids* **35** (1987) 383.
7. M. G. JENKINS, A. GHOSH and A. S. JONATHAN, in "Proceedings of the Society of Experimental Mechanics, Spring Conference on Experimental Mechanics", Albuquerque, USA (1990) p. 179.
8. J. K. WELLS and P. W. R. BEAUMONT, *J. Mater. Sci.*, **20** (1985) 2735.
9. L. S. SIGL and A. G. EVANS, *Mech. Mater.* **8** (1989) 1.
10. H. C. CAO and A. G. EVANS, *ibid.*, **7** (1989) 295.
11. P. G. CHARLAMBIDES and A. G. EVANS, *J. Am. Ceram. Soc.* **72** (1989) 746.
12. A. SHUKLA and S. K. KHANNA, in "Proceedings of the Society of Experimental Mechanics, Spring Conference on Experimental Mechanics", Albuquerque, USA (1990) p. 607.
13. G. R. IRWIN, "Series Representation of the Stress Field Around Constant Speed Cracks," University of Maryland Lecture Notes (1980).
14. R. J. SANFORD and J. W. DALLY, *Eng. Fract. Mech.* **11** (1979) 621.

Received 12 November 1991
and accepted 19 November 1992